JOURNAL OF MATERIALS SCIENCE 28 (1993) 445–453

Transient creep behaviour of hot isostatically pressed silicon nitride

S. M. WIEDERHORN, B. J. HOCKEY, D. C. CRANMER
National Institute of Standards and Technology, Gaithersburg, MD 20899, USA
R. YECKLEY
Norton/TRW Ceramics, Goddard Road, Northboro, MA 01532, USA

Transient creep is shown to dominate the high-temperature behaviour of a grade of hot isostatically pressed silicon nitride containing only 4 wt% Y_2O_3 as a sintering aid. Contributing factors to transient creep are discussed and it is concluded that the most likely cause of long-term transient creep in the present study is intergranular sliding and interlocking of silicon nitride grains. In early stages of creep, devitrification of the intergranular phase, and intergranular flow of that phase may also contribute to the transient creep process. The occurrence of transient creep precluded the determination of an activation energy on the as-received material. However, after creep in the temperature range 1330–1430 °C for times exceeding approximately 1100 h, an apparent activation energy of $\approx 1260\ kJ\ mol^{-1}$ was measured. It is suggested that the apparent activation energy for creep is determined by the mobility and concentration of diffusing species in the intergranular glassy phase. The time-to-rupture was found to be a power function of the minimum strain rate, independent of applied stress or temperature. Hence, creep–rupture behaviour followed a Monkman–Grant relation. A strain rate exponent of -1.12 was determined.

1. Introduction

Because silicon nitride is a material that does not sinter easily in the "pure" state, additives such as Y_2O_3, MgO, and Al_2O_3, or a mixture of these are used to promote liquid-phase sintering [1, 2]. The retained intergranular vitreous phase inherent in this process effectively controls high-temperature behaviour. At elevated temperatures, the intergranular glass softens, allowing creep deformation to occur. Eventually, the material fails as a consequence of the creep process.

The vitreous bonding phase is not stable at elevated temperatures (largely as a consequence of devitrification) and so its flow and transport properties change with time. Consequently, the creep and creep–rupture behaviour of Si_3N_4 also change as a function of time. Because it seems unlikely that fully dense, high-toughness silicon nitride will be made economically without an intergranular vitreous phase, research efforts are being directed towards improving the stability and refractoriness of that phase. Methods of design are also being developed to account for transient creep resulting from microstructural instability at elevated temperature.

This paper deals with one of the newer grades of silicon nitride, NT154 (Norton/TRW Co.), a commercial grade of hot isostatically pressed (HIPed) material processed with ≈ 4 wt% Y_2O_3 as a sintering aid. At room temperature, this material has a toughness of $\approx 6\ MPa\ m^{1/2}$ and a strength of ≈ 700 MPa [3]. At 1300 °C its tensile strength is ≈ 400 MPa [3]. The material also has excellent creep resistance at elevated temperatures [4].

In this work, the tensile creep and creep–rupture behaviour of NT154 were examined further. In particular, it has been shown that over the temperature range 1330–1430 °C, the material exhibits transient tensile creep behaviour, in that the strain rate continuously decreases with time. Such transient creep behaviour complicates methods of lifetime prediction, which traditionally relate lifetime to "steady state" strain rate. While the underlying causes of long-term, transient creep cannot yet be fully explained, microstructural analyses of NT154 indicate that this behaviour ultimately relates to both the initial microstructure and to changes in microstructure that occur during creep at elevated temperatures. In this regard, microstructure is shown to have a profound effect on the process of cavitation, which occurs during tensile creep.

2. Experimental procedure

Both the specimen design and the test apparatus used in this tensile creep study have been previously described [5]. In brief, this apparatus uses flat dog-bone shaped samples to which SiC "flags" are attached to define the gauge length. During tensile testing, relative displacements of the flags are continuously monitored by a laser extensometer to an accuracy of $\pm 2\ \mu m$ at temperature. To ensure thermal stability, the specimens were maintained at the test temperature for

0022–2461

approximately 20 h before testing. Tests were made over a temperature range 1330–1430 °C and a stress range of 75–150 MPa. For most tests, the applied stress was maintained until the specimen failed. In this way, both the creep and creep–rupture behaviour of the material could be characterized.

The microstructure of tested specimens was studied by transmission electron microscopy (TEM). TEM sections were taken from the gauge section after the conclusion of most tests. To differentiate between the effects of creep and annealing on the microstructure, these TEM sections were compared with TEM sections from the unstressed ends of selected tensile specimens and with TEM sections from as-received material. Microstructural analyses were conducted on specimens that failed during creep (4–256 h exposure) and on specimens from tests that were interrupted before failure (exposure times ranging from $\approx$1000–$\approx$4500 h). Specimens from interrupted tests were cooled under load to prevent stress relaxation. The gauge sections of crept specimens were cut parallel to the stress axis to obtain both near-surface and mid-plane TEM sections. Prior to final preparation, these sections were examined optically for evidence of distributed creep cavitation or crack damage.

3. Results

3.1. Microstructural analysis

Representative views of the microstructure of the as-received material are shown in Fig. 1. In this material, the silicon nitride grains varied in both size and morphology, but were invariably β-phase. Grain shapes tended to be either equiaxed or acicular, Fig. 1. The equiaxed grains had dimensions either in the submicrometre range or in the 2–3 μm range. The acicular grains were usually 1–6 μm long with widths of 1 μm or less. Presumably, this composite-like microstructure resulted from limited grain growth during processing. Continued β-Si_3N_4 grain growth during prolonged tensile testing at $\approx$1330 – 1430 °C was not apparent.

In the as-received state, most multi-grain junctions were found to contain intergranular glass, which on

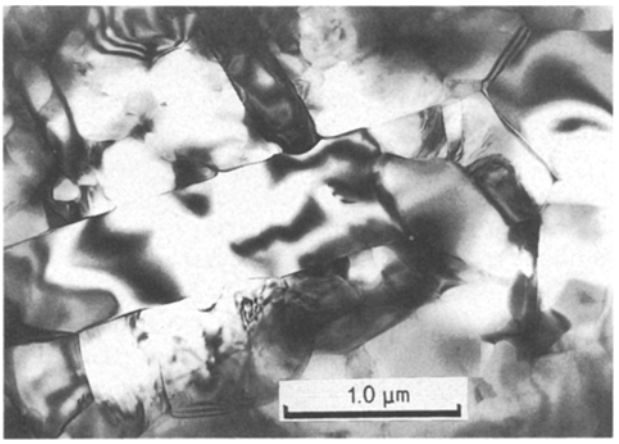

Figure 1 Representative view of microstructure showing variable size and morphology of β-Si_3N_4 grains.

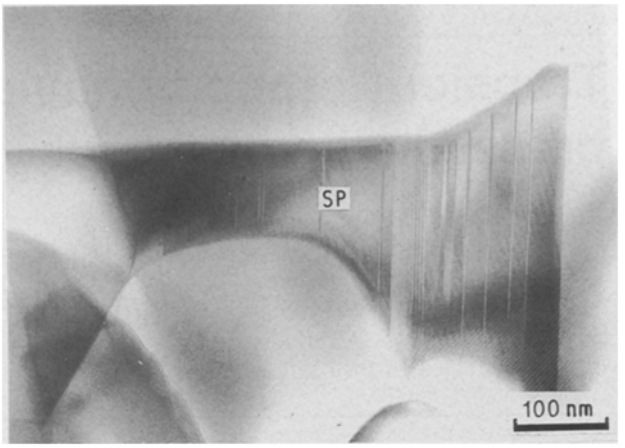

Figure 2 During creep, devitrification of intergranular glass contained within multi-grain junctions results in the formation of crystalline secondary phases (SP), identified as either α-$Y_2Si_2O_7$ (as illustrated here) or *N*-apatite (an yttrium-silicon oxynitride).

the basis of an energy dispersive spectroscopy (EDS) analysis appeared to be an yttrium silicate glass having a composition by weight of roughly 0.6 Y_2O_3 and 0.4 SiO_2. Some of the multi-grain junctions, however, also contained clusters of small (< 100 nm) secondary-phase crystallites, indicating the initiation of glass devitrification during cool-down from the processing temperature.

During creep, devitrification occurs rapidly, resulting in nearly complete crystallization of the glass contained within the multi-grain junctions throughout the sample, Fig. 2. Identification of the secondary phases by electron diffraction and energy dispersive spectroscopy revealed the exclusive formation of either α-$Y_2Si_2O_7$ (triclinic yttrium disilicate) or N-apatite (a hexagonal yttrium-silicon oxynitride). Importantly, no apparent difference was found in either the extent or nature of multi-grain crystallization after test times ranging from 4 to over 4000 h. As such it appears that devitrification of the bulk of the intergranular glass originally contained within NT154 occurs rapidly at the test temperatures and is complete prior to loading.

Despite the rapid crystallization of multi-grain junctions, complete devitrification of the intergranular glass was never observed. Regardless of the time at temperature, residual yttrium silicate glassy interfaces of various thickness ($\approx$1–10 nm) separated the various secondary phases from adjacent silicon nitride grains, Fig. 3a. Similarly, examination of the narrow interfaces separating adjacent silicon nitride grains by a variety of techniques (high-resolution or diffuse dark-field imaging together with EDS) indicates that most of these interfaces contain residual glass. These interfaces are generally irregular, exhibiting gradual or abrupt changes in both orientation and apparent thickness. In this regard, interfacial widths ranged from roughly 0.5–2 nm; a value of $\approx$1 nm is considered representative for this material, Fig. 3b. (On the basis of current results, no attempt is made to establish a lower limit to interfacial glass thickness or to establish the occurrence of "true contact".).

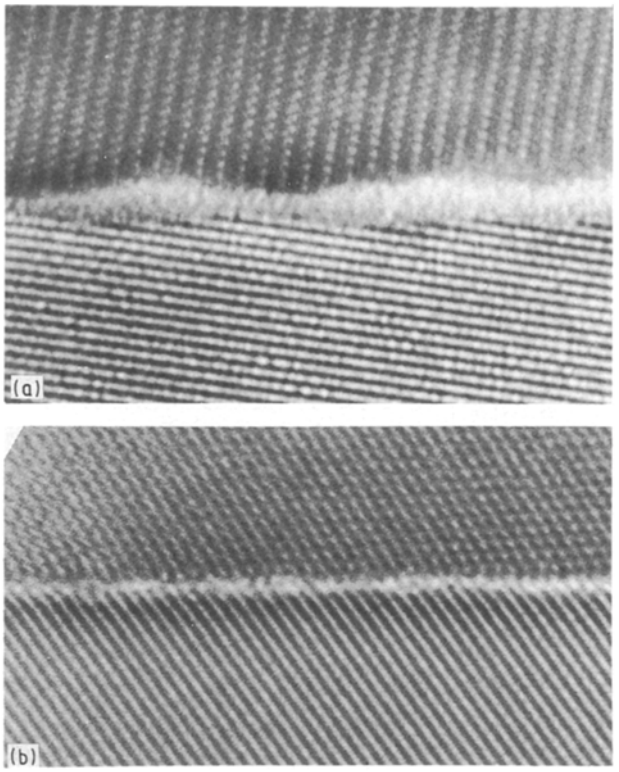

Figure 3 Representative views of glassy interfaces separating (a) α-$Y_2Si_2O_7$ secondary phase (top) and matrix β-Si_3N_4 grain (bottom). Fringe spacing in Si_3N_4 (bottom) = 0.66 nm; (b) adjacent Si_3N_4 grains. Fringe spacing in bottom Si_3N_4 = 0.66 nm.

Devitrification does not eliminate the glassy interfaces in this material. Nevertheless, the rapid crystallization of much of the original glass will necessarily alter the composition of retained interfacial glass. While the composition of the residual glass within these narrow interfaces could not be determined directly by EDS, the relative shift in yttrium to silicon ratio can be deduced by comparing the composition of the original glass to that of the primary products of devitrification. In this comparison, the Y/Si ratio for both $Y_2Si_2O_7$ (3.2) and *N*-apatite (5.3) are larger than that of the original glass (2.5), indicating a relative depletion of yttria, or, alternatively, an enrichment of silica upon devitrification.

From the phase diagram published by Gauckler *et al.* [6], the Y/Si ratio of the eutectic liquid is 2.6, which is close to that of the as-received material. As the glass is the only source of yttrium, this ratio has to decrease as the glass devitrifies. Direct evidence for a decrease in the yttria concentration upon annealing was obtained by Wilkinson *et al.* [7] on a grade of Si_3N_4 containing both yttria and alumina as sintering aids. Considering the extent of devitrification, the associated change in residual glass composition should be sufficient to alter the glass properties and, hence, creep resistance. Moreover, while devitrification occurs rapidly, equilibration of the glass composition may require longer periods and, hence, may contribute to transient creep behaviour.

More generally, transient creep in this material appears to be a consequence of the effect of microstructure on deformation. The narrow and highly irregular glassy interfaces restrict interfacial sliding and the redistribution of interfacial glass by viscous flow. As a consequence, deformation will be inhomogeneous and relative displacements of adjacent grains will be physically limited by grain-to-grain contact. Evidence for distributed grain-contact sites is obtained by the observation of localized "strain whorls" in crept samples cooled under load, Fig. 4. These strain whorls appear to be located primarily on interfaces that are roughly parallel to the tensile stress axis. These contact sites on the interfaces will impede grain displacement and can lead to transient creep behaviour if the area of contact increases as a function of time. During the creep process, these stresses are probably relieved by diffusional transport, in a manner originally described by Raj and Ashby [8].

The effect of microstructure on creep behaviour is, perhaps, most clearly reflected in the nature of the cavitation process that occurs in this material. For NT154, tensile creep at 1330–1430 °C results in the formation of isolated ellipsoidal shaped cavities, Fig. 5, which are preferentially distributed on tensile-oriented interfaces separating adjacent Si_3N_4 grains. Regardless of test conditions, all samples contained distributions of such cavities, typically with major axis dimensions of 50–300 nm and aspect ratios of 2 or 3 to 1. Because the interface widths are typically 1–2 nm or less, cavity growth clearly involves diffusive growth of the cavities into the silicon nitride grains, probably by a Hull–Rimmer type of mechanism [9]. Silicon nitride leaves the cavitated area by surface diffusion, travels through the grain-boundary phase and then plates out along the interface. (Diffusion is probably not by molecular motion of Si_3N_4, but by ionic motion of silicon and nitrogen ions.) This mechanism is consistent with the micrograph in Fig. 5. Thus, the cavitation process in this material provides clear evidence for the operation of localized diffusive transport processes at the test temperatures used in the present study.

Cavitation in NT154 can be contrasted with other grades of silicon nitride in which cavities are contained within the residual vitreous interface and grow along

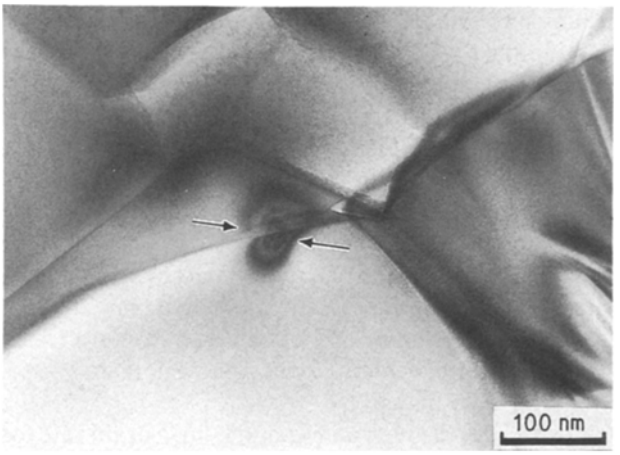

Figure 4 Localized strain contrast contours ("strain whorls") at interface between Si_3N_4 grains indicative of residual stresses due to grain-to-grain contact. Note, arrows pointing to site of contact are anti-parallel to direction of tensile stress. Such strain contrast contours were first reported by Lange *et al.* [31].

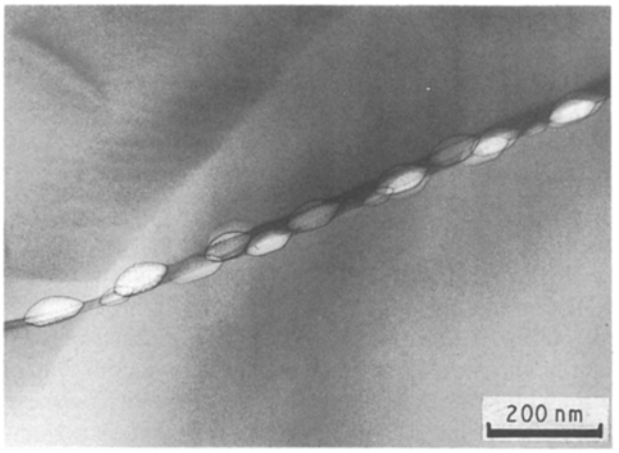

Figure 5 Isolated, ellipsoidal-shaped cavities typically produced within narrow interfaces between Si_3N_4 grains during tensile creep. Note cavity widths exceed the thickness of the interface, which is inclined to the plane of view, and results in apparent cavity overlap.

the interface to form creep crack nuclei [10]. In NT154, no evidence was found for full-facet cavity growth or even for interactive growth of the individual cavities. Creep crack initiation thus appears to require a critical density of interfacial cavities. Lack of evidence for distributed creep cracks within the samples further indicates that rupture occurs by rapid crack growth once a critical nucleus is formed. Thus, lifetime seems to be determined primarily by the time for crack nucleation.

3.2. Creep behaviour

An important characteristic of the silicon nitride studied in this paper is the occurrence of transient creep for all conditions of testing. This behaviour is illustrated in Fig. 6 for three specimens: one that failed in 4 h, one that failed in 244 h and one that survived for over 4500 h. As can be seen, each plot of strain versus time exhibits curvature, indicating that creep rate continuously decreases as a function of time. True steady state creep does not appear to occur for this material.

Transient creep obviously decreases our ability to characterize the effect of temperature and stress on strain rate. Fig. 7a and b summarize test results on the effect of temperature on creep rate. Data for both figures were obtained from a single test specimen. The stress on the specimen was held constant (100 MPa), while the temperature was changed over the range 1330–1430 °C. In Fig. 7a, strain is plotted against time to illustrate the marked change in creep behaviour with temperature; for each test interval, the temperature and final strain rate are indicated. Note that the sequence of tests involves both increases and decreases in temperature. Although the time intervals varied, none was less than 100 h.

In Fig. 7b, the natural log of the final strain rate for each interval is plotted as an inverse function of temperature; each data point is numbered to show the sequential order of temperature change. Taken in sequence, the data in this Arrhenius plot approach a single curve only after ≈ 1100 h of testing. Data points

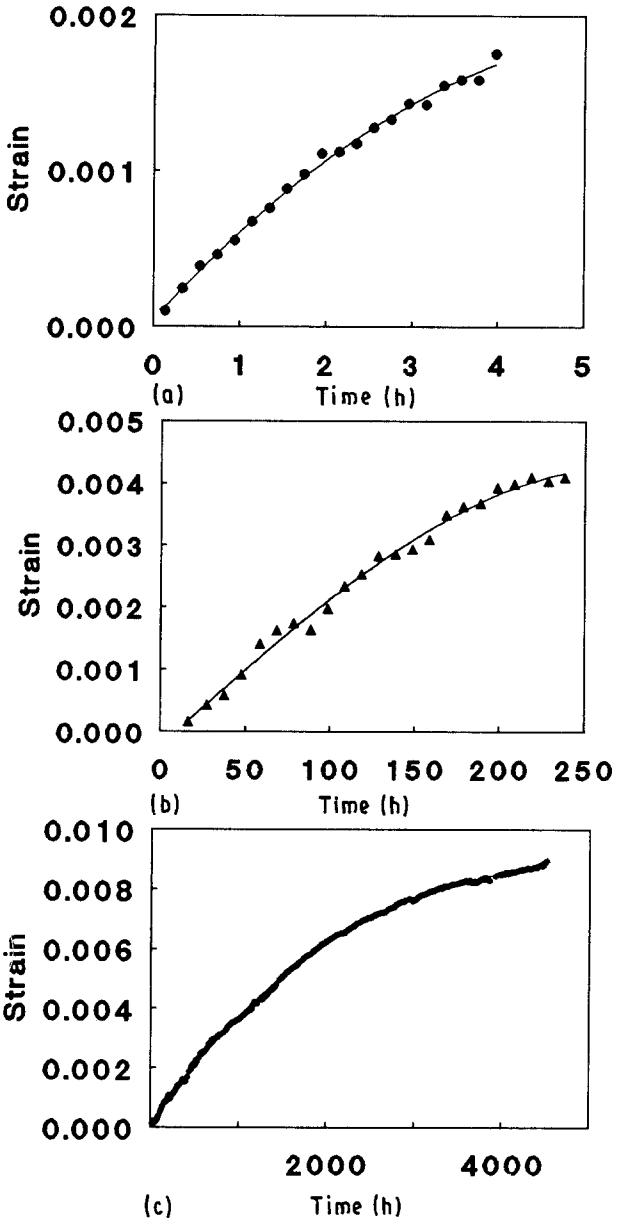

Figure 6 Typical creep curves for NT154: (a) 4 h lifetime, 1385 °C, 150 MPa; (b) 244 h lifetime, 1385 °C, 100 MPa; (c) > 4500 h lifetime, 1370 °C, 75 MPa. Regardless of the test period, transient creep occurs over the entire curve. The curvature is particularly apparent for the longer test period.

4–7 cluster about a straight line, whereas data point 1 lies some distance from the line. A linear fit of data points 4–7 yields a value of ≈ 1260 kJ mol^{-1} for the apparent activation energy. Physical significance is attached to the dependence defined by data points 4–7, because the linear fit here is relatively unaffected by the sequential order, total time, or whether the temperature was raised or lowered. The significance of the apparent activation energy for creep is discussed below.

Efforts to determine the stress dependence for the creep rate were complicated not only by transient behaviour, but by specimen rupture. The strong dependence of specimen lifetime on stress severely limited our ability to obtain data at fixed times or fixed strains. Nevertheless, by plotting the logarithm of the minimum creep rate as a function of the logarithm of the applied stress, a measure of the stress sensitivity of

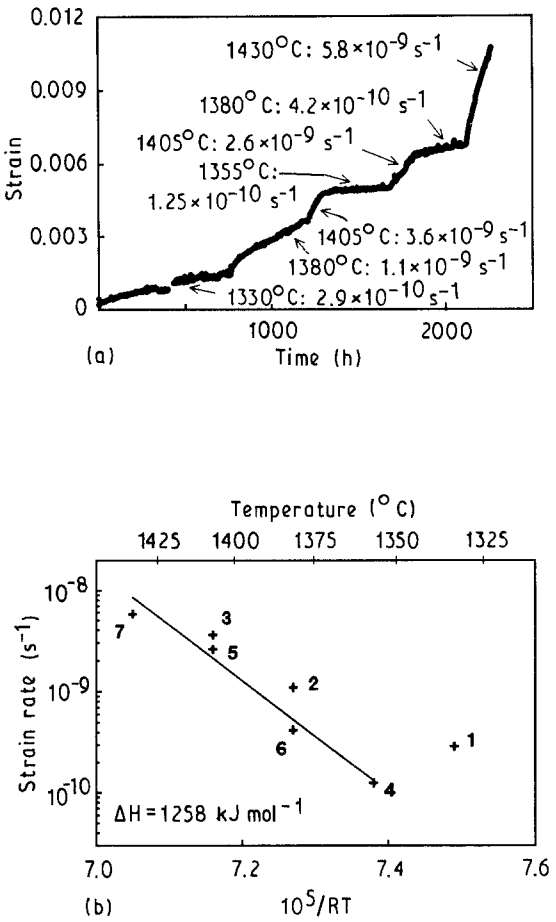

Figure 7 Effect of temperature on the creep of NT154: (a) strain as a function of exposure time; (b) minimum creep rate as a function of temperature. Transient creep effects are evident for the time required for the data to approach a common Arrhenius curve. Approximately 1100 h creep were required to approach a semblance of steady state creep. Stress: 100 MPa.

the creep behaviour of this material is obtained, Fig. 8. A power-law fit with an exponent of 6.9 was determined from the data at 1385 °C. The stress dependence of the creep data is similar to that measured in other studies of the creep of Si_3N_4 [10, 11]. In other structural ceramics, high values of the stress exponent have been associated with cavitation [12, 13]. Because cavitation is observed in the present study, it is possible that the high value of the creep exponent in this paper is also a consequence of creep cavitation, or some process associated with the cavitation.

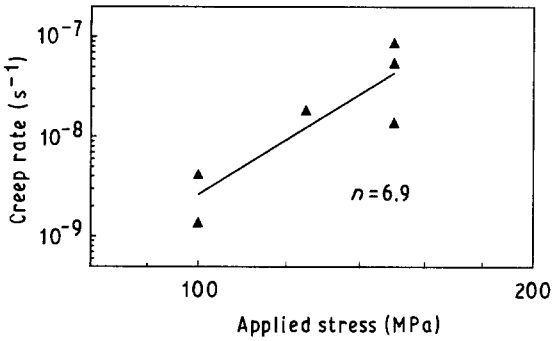

Figure 8 Stress sensitivity of the creep rate of NT154. Tests were conducted at 1385 °C.

3.3. Creep–rupture behaviour

Rupture data collected in this study can be represented by a Monkman–Grant [14] diagram, in which the logarithm of the time to failure, t_f, is plotted as a function of the logarithm of the minimum creep rate, $\dot{\varepsilon}_{min}$, Fig. 9. In this figure, failure times ranged from 4 – 256 h. Runs that were discontinued are also plotted with small arrows next to the plotting symbol (squares).

The strain rate exponent, m, of the Monkman–Grant curve has a value of about -1.12. (A power law equation was used to relate the rupture time, t_f, to the creep rate, $\dot{\varepsilon}$: $t_f = B\dot{\varepsilon}^m$. This equation was first used by Monkman and Grant [14] to describe the creep rupture of high-temperature alloys.) All of the rupture data fell close to a single curve, regardless of applied stress or temperature. Accordingly, the lifetime of NT154 appears to be determined solely by the creep behaviour of the solid: the higher the creep rate, the shorter the lifetime. Apparently, the lifetime of silicon nitride can be improved by enhancing its creep resistance. Methods of improving creep resistance include increasing the effective viscosity of the intergranular phase, decreasing the amount of intergranular phase and increasing the grain size of the solid. The first two of these have proved especially effective in improving the creep resistance of structural ceramics [15–18].

4. Discussion

4.1. Creep

4.1.1. Previous studies

The results of this study substantiate previous reports of transient tensile creep behaviour in silicon nitride. In an early study of the creep of a magnesia-doped grade of hot-pressed silicon nitride (NC132), Arons and Tien [19] found no evidence of steady state creep for tests lasting as long as 405 h and strains up to

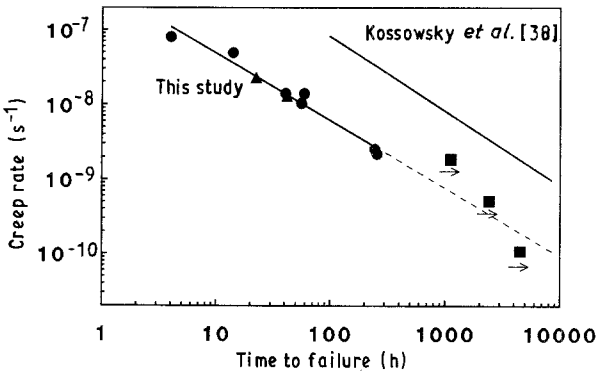

Figure 9 Creep rupture data: minimum creep rate as a function of the time to failure. The circles indicate as-received specimens that failed under load; the triangles indicate two specimens annealed at 1350 °C for 500 h before testing; the arrows indicate specimens that were interrupted before failure. Tests were conducted at 1350 and 1375 °C and stresses that ranged from 75–150 MPa. Although the data set is limited, the time-to-failure seems to be determined uniquely by the rate of creep in this material, suggesting that improvement of the creep rate is of paramount importance to improving lifetime.

2.25%. The strain was found to be a power-law function of time. An activation energy of about 848 kJ mol^{-1} and a stress exponent of 4 was obtained by these authors. Transient creep behaviour was attributed to the flow of glass from between grains and the gradual transfer of load from the glassy interphase to the grains. This mechanism is somewhat similar to that proposed earlier by Lange [20]. As TEM studies were not conducted on their materials, the role of devitrification of the intergranular glassy phase was not considered.

In a recent study by Hockey *et al.* [10] on the tensile creep of a grade of Si_3N_4 containing 6 wt % Y_2O_3 and 1.1 wt % Al_2O_3, transient creep was also found to occur over prolonged test periods. This transient behaviour was attributed to an effective work hardening caused by progressive devitrification of intergranular glass. As in the present study, devitrification never completely eliminated the retained glass phase. It did, however, substantially reduce the amount of glass, and also caused significant changes in the composition of the glass. Devitrification occurred more gradually than that observed in NT154, and resulted in a retained interfacial silica glass depleted in Y_2O_3, but enriched in Al_2O_3. Long-term preannealing (to cause extensive devitrification) resulted in significant increases in creep resistance, but did not eliminate transient behaviour. As devitrification of residual glass was never complete, transient creep was assumed to be due to a gradual increase in the glass viscosity with continuous changes in composition.

In another recent study on silicon nitride, containing both yttria and magnesia as sintering aids, Gürtler and Grathwohl [21] obtained tensile creep curves similar to those presented here. In their study, work hardening was attributed to a gradual increase in refractoriness of the bonding phase caused by the migration of impurities and cations (Y_2O_3 and MgO) from the intergranular glass to the surface oxide layer. Thus, the intergranular glass composition was changed by selective migration of cations to the surface oxide layer in a manner that is similar to that proposed by Clarke and Lange [22].

4.1.2. Models of creep

Clearly both devitrification and surface oxidation occur in silicon nitride, resulting in composition changes in the residual glass during high-temperature creep tests. The importance of these composition changes can be rationalized on the basis of two generalized creep models for two-phase solids. Both models assume a structure of relatively rigid grains held together by a softer viscous phase, Fig. 10. In the first model, only the viscous phase deforms under stress. While the grains cannot change shape, relative displacements between the grains can occur. These displacements are accommodated by flow in the viscous phase, from high- to low-pressure grain interfaces. This model of creep was first proposed by Drucker [23] and later by Lange [20]. The model has recently been extended by Dryden *et al.* [24] and Debschütz *et al.* [25] to consider transient creep behaviour. On the basis of these viscous flow models, the microstructural parameters controlling creep are grain size, d, bonding phase thickness, w, and the effective viscosity, η, of the bonding phase. The functional dependence of the strain rate, $\dot{\varepsilon}$, on these parameters is given by

$$\dot{\varepsilon} = \alpha_1 \sigma (w/d)^3/\eta \quad (1)$$

where σ is the applied stress, and α_1 and α_2 are non-dimensional constants.

The second model for creep assumes that grain-to-grain contact sites are present or develop during deformation. Creep deformation is thus governed by stress-enhanced dissolution of the contact sites. In this model, the viscous phase acts as a medium through which material is transported from high stress contact sites to low stress surfaces where precipitation occurs. This diffusion model of deformation was originally proposed by Coble [26] to take into account enhanced diffusion along grain boundaries. Since then, it has been modified by Raj [27] and by Pharr and Ashby [28], and is now commonly referred to as solution-reprecipitation. Based on this model, the creep rate is again expressed in terms of grain size, d, bonding phase thickness, w, and the viscosity of the bonding phase, η. However, the functional dependence of strain rate, $\dot{\varepsilon}$, on these parameters is different from that expressed in Equation 1

$$\dot{\varepsilon} = \alpha_2 w \sigma \, \Omega^{2/3}/d^3\eta \quad (2)$$

where Ω is the molar volume of the diffusing species. The Einstein–Stokes equation [29] is used to relate diffusivity to viscosity.

From Equations 1 and 2, both models of creep predict an inverse dependence of strain rate on viscosity. Thus, time-dependent changes in the composition of the viscous phase that result in increased viscosity will lead to a time-dependent decrease in the strain rate. Hence, devitrification of the bonding phase in the silicon nitride should have a significant effect on the creep behaviour of this material. The role of viscosity of the vitreous phase has also been demonstrated for vitreous bonded alumina [30].

Equations 1 and 2 also suggest that time-dependent changes in grain separation or in grain size can result in transient creep behaviour. Thus, if the thickness of interfaces between grains is decreased as a consequence of the creep process, the creep rate will decrease. Furthermore, because the stress in Equations 1 and 2 is the local stress, not the applied stress, any process that leads to a time-dependent change in local stress will also result in a change in creep rate. As an example, if solution-reprecipitation were the controlling creep mechanism, and the contact area between grains increased as a consequence of the creep process, then the local stress and, therefore, the rate of creep will decrease as a function of time. As discussed below, this may be one of the important mechanisms accounting for primary creep in the present study.

Dryden *et al.* [24] recently extended the treatment of creep by viscous flow, i.e. Equation 1, to account for transient behaviour and for differences in tensile and

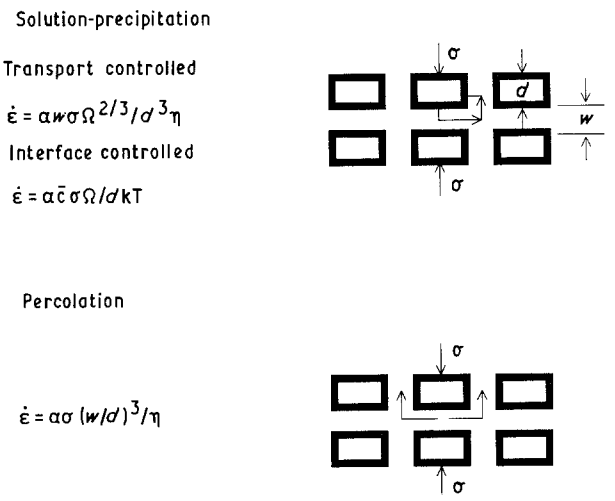

Figure 10 Models of two-phase creep: solution–precipitation; percolation. In the equations given above: α is a dimensionless constant (different for each equation); Ω is the molar volume of the grains; k Boltzmann's constant; η the viscosity of the bonding phase; c the surface dissolution velocity under a unit driving force. After Pharr and Ashby [28]

compressive creep. In their analysis, transient behaviour during viscous flow develops as a consequence of changes in grain-separation distance with increased strain. The idea behind the treatment is straightforward. In the initial stages of deformation, flow of fluid between the grains changes the width of the intergranular spacing locally. In tension, the separation between grain surfaces that lie normal to the applied stress increases, whereas separation between grain surfaces that lie parallel to the applied stress decreases. The opposite holds true for compression.

The rate of fluid flow, and hence the rate of creep is determined primarily by the more narrowly spaced grains. Therefore, as the separation between grains decreases, flow becomes more difficult (in both tension and compression) and the creep rate decreases, resulting in transient creep behaviour. Transient creep in tension and compression differ because there are twice as many grain interfaces (and hence twice as much fluid) parallel to the applied stress. With time, the interfacial spacing decreases sufficiently that some of the grains come into contact, reducing the amount of deformation that can occur. Strain whorls between Si_3N_4 grains, Fig. 4, lend credence to the possibility of contact between grains during deformation. Such strain whorls were first reported by Lange *et al.* [31] in compressive creep studies on MgO-doped, hot-pressed Si_3N_4 and more recently by Quinn and Braue [32] in flexural creep studies of sintered silicon nitride.

In a regular structure such as that depicted in Fig. 10, deformation is homogeneous, and contact between grains will occur simultaneously throughout the structure. Under such idealized conditions, Dryden *et al.* [24] predict the contact limit in tension as $\varepsilon = w/d$. Applying this equation for NT154, with $w \approx 10^{-3}$ μm and $d \approx 1$ μm, grain contact should occur when $\varepsilon \approx 10^{-3}$. This strain limit is far below the strains of 0.005–0.091 typically realized during tensile creep testing. This finding suggests that deformation by grain-boundary sliding and flow of material is important only in the early stages of the creep process. Contact between grains occurs relatively early in that process and as contact between grains is established, other mechanisms of deformation control the creep behaviour.

The observation of cavities on tensile boundaries of all specimens tested suggests that cavitation, or processes associated with cavitation, play an important role in the mechanism of deformation as creep continues. Cavitation relieves the internal stresses that build up as a consequence of fluid flow and grain-boundary sliding, so that creep deformation can continue even after firm contact between grains has occurred. The creep rate is then controlled either by the rate of cavity nucleation and growth, or by the rate of sliding of the grain boundaries, whichever process is slower.

Cavitation control of the creep rate is unlikely to provide an acceptable explanation for the transient creep observed in the present set of experiments. When cavitation controls creep, creep rates are expected to increase with time as the number and size of cavities in the gauge section increase. The reason for this acceleration in the creep rate is that cavity formation reduces the cross-section of the specimen that is available to carry the load, and, therefore, increases the local stress that drives the creep process. The idea that cavitation enhances creep rate provides a ready explanation for the phenomenon of tertiary creep in metals [33], but is unlikely to provide an explanation for the work hardening observed in the present experiment.

Based on the above discussion, we feel that the transient creep reported in this paper was primarily a consequence of intergranular contact as the grains of silicon nitride slid over one another. Because the grain boundaries in the silicon nitride are not flat and smooth, they become interlocked as grain-boundary sliding occurs. Contact is made either at curved surfaces or at steps on these surfaces. In this way, stresses released due to cavitation on surfaces that are primarily normal to the applied stress are picked up by the sliding boundaries. The role of grain-boundary steps or curved surfaces in impeding grain-boundary sliding and in nucleating cavities is widely accepted in materials literature [34, 35]. Recently, this mechanism of deformation has been used by Chan *et al.* [36] to understand creep-cavity formation in ceramic materials.

Models of grain-boundary sliding [8] are usually based on assumptions that lead to steady state creep, so some modification of these models is needed to explain transient creep. Qualitatively, transient creep can be understood if the real area of contact between grains increases as grain-boundary sliding occurs, for then the local stresses at contact sites will decrease during sliding. The actual process of sliding is probably controlled locally by a solution-reprecipitation mechanism, such as that suggested by Raj and Ashby [8]. In this scenario of the creep behaviour, the rate of cavity formation and growth is constrained by the rate at which grain-boundary sliding occurs. The observation of strain whorls on boundaries that are parallel to

the applied stress provides partial support for this description of transient creep behaviour. Also, the fact that cavity formation in this material occurs by a diffusional process is evidence that solution–reprecipitation can occur at grain boundaries during creep. Detailed mechanisms for such a process have yet to be worked out.

4.2. Activation energy

The activation energy measured in the current experiment, $\approx 1260\,kJ\,mol^{-1}$ is higher than that reported on other grades of silicon nitride, 600–700 $kJ\,mol^{-1}$ [21, 37, 38]. Values approaching that reported here, however, have been measured recently by Ohji [39] and by Ferber and Jenkins [40] in an investigation of the tensile creep behaviour of silicon nitride. Ohji studied a grade of silicon nitride containing 5 wt % Y_2O_3 and 3 wt % Al_2O_3. Activation energies for whisker-free and 20 wt % SiC whisker-reinforced material were 1190 and 1065 $kJ\,mol^{-1}$, respectively. Ohji also reported long-term transient creep behaviour for these materials.

Ferber and Jenkins [40] studied the tensile creep behaviour of a grade of HIPed silicon nitride that contained 6% Y_2O_3. They measured an activation energy of 1100 $kJ\,mol^{-1}$ and a stress exponent of 5, both of which are consistent with values reported in this study. Based on our results and those reported by Ohji, and by Ferber and Jenkins, we suspect that these high values of the apparent activation energy are not experimental accidents, but reflect real processes occurring during deformation.

If, as suggested above, solution–reprecipitation at intergranular contact sites plays a major role in the deformation process, then diffusive transport along the grain interfaces will also be important to the creep process. As noted by Raj and Morgan [41], such transport processes often depend on a number of different factors that determine the apparent activation energy. The rate of creep will depend on the rate of transport of silicon nitride along the grain interface, which in turn depends on the mobility and concentration of the silicon nitride in the glass at the interface. The temperature dependence of the mobility and the concentration together determine the measured value of the apparent activation energy.

In their discussion of the reasons for the high activation energies for creep, densification and grain-boundary sliding in hot-pressed silicon nitride, Raj and Morgan [41] suggest that the Gibb's free energy controlling the concentration of silicon nitride in the interfacial glass of a magnesia-doped silicon nitride was approximately equal to the heat of solution of the silicon nitride in the glass, ΔH_s. From densification experiments reported by Bowen *et al.* [42], they estimate the heat of solution as $\Delta H_s = 400\,kJ\,mol^{-1}$. The temperature dependence of the mobility can be estimated from the activation energy for the viscosity of oxynitride glasses (assuming the applicability of the Stokes–Einstein equation). Rouxel *et al.* [43] measured the viscosity of an oxynitride glass (Y 17.3, Si 34.7, Al 9.9, O 31.9, N 6.2 wt %) over the temperature range 850–980 °C. The activation energy for viscosity ranged from $335\,kJ\,mol^{-1}$ at 880 °C to about $1000\,kJ\,mol^{-1}$ at 940 °C, and slowly decreased to $850\,kJ\,mol^{-1}$ at 980 °C. These values were consistent with measurements by Hampshire *et al.* on a similar glass [44]. If oxynitride glasses containing only yttria behave in a similar manner, then the activation energy for viscosity plus the heat of solution of silicon nitride in glass are sufficient to account for the high activation energy, $1260\,kJ\,mol^{-1}$, for creep measured in the current study.

4.3. Creep–rupture

The Monkman–Grant representation of creep–rupture behaviour was first applied to silicon nitride (HS130, a magnesia-doped material) by Kossowsky *et al.* [38], who showed that the strain exponent of the Monkman–Grant curve had a value of -1 compared to -1.12 in the present study, Fig. 9. The two sets of data are displaced from one another, with HS130 exhibiting a factor of ≈ 10 increase in time-to-failure compared to NT154 at the same strain rate. The NT154 is, however, so much more creep resistant than the HS130, that at a given stress the failure time of the NT154 is several orders of magnitude greater than that of the HS130. For example, at 1385 °C and 70.5 MPa the HS130 creeps at a rate of $\approx 4.7 \times 10^{-7}\,s^{-1}$ [38], while at the same temperature and stress, the NT154 creeps at a rate of $\approx 3.5 \times 10^{-10}\,s^{-1}$. Referring to the Monkman–Grant curves for these materials, the expected lifetime of the NT154 is ≈ 2500 h, while that for the HS130 is ≈ 18 h. Thus, the greater resistance of NT154 to creep makes it the superior material with regard to failure by creep–rupture.

In earlier studies [10, 45, 46], we noted that when stress–rupture data cluster along a single curve on a Monkman–Grant plot, as in Fig. 9, then the temperature and stress dependence of the creep–rupture behaviour are determined primarily by the temperature and stress dependence of the creep behaviour. This is easily demonstrated [45]. Using the power-law expression for the time to failure, $t_f = A\dot{\varepsilon}^m$ and an

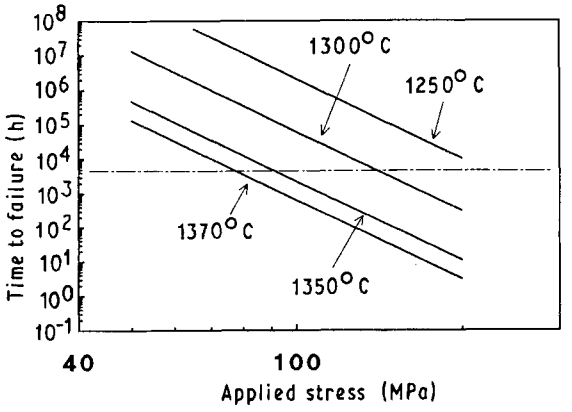

Figure 11 Lifetime prediction based on creep and creep–rupture data. This graph is calculated from the creep, Figs. 6 and 7, and creep rupture, Fig. 8, data collected on NT154. (– – –) 1 year lifetime. After Cranmer *et al.* [46].

expression for the creep rate as a function of applied stress, $\varepsilon = B\sigma^n \exp(-\Delta H/RT)$, a combined stress–rupture formula can be derived: $t_f = AB^m \sigma^{mn} \exp(-m\Delta H/RT)$. Using this expression, preliminary lifetime predictions for NT154 have been made [46], Fig. 11. The horizontal line in the figure represents 1 year of lifetime. As can be seen, the maximum stress allowed for the material depends on the service temperature. At the temperature of 1370 °C (the maximum anticipated temperature for this material) and an anticipated lifetime of 1 year, a stress of 80 MPa is estimated for NT154.

Acknowledgement

This work was supported by the US Department of Energy, Ceramic Technology for Advanced Heat Engines Program under Interagency Agreement DE-AI05-850R21569.

References

1. G. ZIEGLER, J. HEINRICH and G. WÖTTING, *J. Mater. Sci.* **22** (1987) 3041.
2. F. F. LANGE, *Int. Metals Rev.* **1** (1980).
3. N. L. HECHT, S. M. GOODRICH, L. CHUCK, and D. E. McCULLUM, in "Annual Automotive Technology Development Contractors' Coordination Meeting", 22–25 October 1990, pp. 199–212.
4. K. C. LIU, H. PIH, C. O. STEVENS and C.R. BRINKMAN, *ibid.*
5. D. F. CARROLL, S. M. WIEDERHORN, and D. E. ROBERTS, *J. Amer. Ceram. Soc.* **72** (1989) 227.
6. L. J. GAUCKLER, H. HOHNKE and T. Y. TIEN, *ibid.* **63** (1–2) (1980) 35.
7. D. S. WILKINSON, M. CHADWICK and A. G. ROBERTSON, in "Proceedings of the International Symposium on Advanced Structural Materials", Montreal, August 1988 (Pergamon Press, New York, 1989) pp. 131–38.
8. R. RAJ and M. F. ASHBY, *Metal. Trans.* **2** (1971) 1113.
9. D. HULL and D. E. RIMMER, *Phil. Mag.* **4** (1969) 673.
10. B. J. HOCKEY, S. M. WIEDERHORN, W. LIU, J. G. BALDONI and S.-T. BULJAN, *J. Mater. Sci.* **26** (1991) 3931.
11. M. K. FERBER, M. G. JENKINS, and V. J. TENNERY, in "Ceramic Engineering and Science Proceedings", 1990, to be published.
12. D. F. CARROLL and R. E. TRESSLER, *J. Amer. Ceram. Soc.* **72** (1989) 49.
13. S. M. WIEDERHORN, D. E. ROBERTS, T. -J. CHUANG, and L. CHUCK, *ibid.* **71** (1988) 602.
14. F. C. MONKMAN and N. J. GRANT, *Proc. ASTM* **56** (1956) 593.
15. F. F. LANGE, *J. Amer. Ceram. Soc.* **57** (1974) 84.
16. G. E. GAZZA, *ibid.* **56** (1973) 662.
17. M. H. LEWIS, in "Tailoring Multiphase and Composite Ceramics", Materials Science Research Vol. 20, edited by R. E. Tressler, G. L. Messing, C. G. Pantano and R. E. Newnham (Plenum Press, New York, 1986) pp. 713–30.
18. F. F. LANGE, B. I. DAVIS and D. R. CLARKE, *J. Mater. Sci.* **15** (1980) 616.
19. R. M. ARONS and J. K. TIEN, *ibid.* **15** (1980) 2046.
20. F. F. LANGE, in "Deformation of Ceramic Materials", edited by R. C. Bradt and R. E. Tressler (Plenum Press, New York, 1972) pp. 361–81.
21. M. GÜRTLER and G. GRATHWOHL, in "Proceedings of the Fourth International Conference on Creep and Fracture of Engineering Materials and Structures" (Institute of Metals, London, 1990).
22. D. R. CLARKE and F. F. LANGE, *J. Amer. Ceram. Soc.* **63** (1980) 586.
23. D. C. DRUCKER, in "High Strength Materials", edited by V. F. Zackay (Wiley, New York, 1965) pp. 795–833.
24. J. R. DRYDEN, D. KUCEROVSKY, D. S. WILKINSON and D. F. WATT, *Acta Metall.* **37** (1989) 2007.
25. K. -D. DEBSCHÜTZ, R. DANZER and G. PETZOW, in "Ceramics Today – Tomorrow's Ceramics," edited by P. Vincenzini (Elsevier Science, Amsterdam, 1991) pp. 727–36.
26. R. L. COBLE, *J. Appl. Phys.* **34** (1963) 1679.
27. R. RAJ, *J. Geophys. Res.* **87** (1982) 4731.
28. G. M. PHARR and M. F. ASHBY, *Acta Metall.* **31** (1983) 129.
29. J. O'M. BOCKRIS and A. K. N. REDDY, "Modern Electrochemistry", Vol. 1 (Plenum, New York, 1970).
30. S. M. WIEDERHORN, B. J. HOCKEY, R. F. KRAUSE Jr. and K. JAKUS, *J. Mater. Sci.* **21** (1986) 810.
31. F. F. LANGE, B. I. DAVIS and D. R. CLARKE, *ibid.* **15** (1980) 610.
32. G. D. QUINN and W. R. BRAUE, *ibid.* **25** (1990) 4377.
33. M. F. ASHBY and B. F. DYSON, in "Advances in Fracture Research", Proceedings of the 6th International Conference on Fracture, New Delhi, India, 4–10 December 1984, edited by S. R. Valluri, D. M. R. Taplin, P. Ramarao, J. F. Knott and R. Dubey (Plenum Press, New York 1984).
34. H. E. EVANS, "Mechanisms of Creep Fracture" (Elsevier Applied Science, London, 1984).
35. H. RIEDEL, "Fracture at High Temperatures" (Springer-Verlag, Berlin, 1986).
36. K. S. CHAN, R. A. PAGE and J. LANKFORD, *Acta Metall.* **34** (1986) 2361.
37. MARTIN S. SELTZER, *Bull. Amer. Ceram. Soc.* **56** (1977) 418.
38. R. KOSSOWSKY, D. G. MILLER and E. S. DIAZ, *J. Mater. Sci.* **10** (1975) 983.
39. T. OHJI and Y. YAMAUCHI *J. Am. Ceram. Soc.* in press.
40. M. K. FERBER and M. G. JENKINS, *J. Amer. Ceram. Soc.*, **75** (1992) 2453.
41. R. RAJ and P.E. D. MORGAN, *ibid.* **64** (1981) C143.
42. L. J. BOWEN, R. J. WESTON, T. G. CARRUTHERS and R. J. BROOK, *J. Mater. Sci.* **13** (1978) 341.
43. T. ROUXEL, J.-L. BESSON, C. GAULT, P. GOURSAT, M. LEIGH and S. HAMPSHIRE, *J. Mater. Sci. Lett.* **8** (1989) 1158.
44. A. HAMPSHIRE, R. A. L. DREW and K. H. JACK, *J. Amer. Ceram. Soc.* **67** (1984) C46.
45. S. M. WIEDERHORN, B. J. HOCKEY and T.-J. CHUANG, in "Toughening Mechanisms in Quasi-Brittle Materials", edited by S. P. Shah, (Kluwer Academic, 1991).
46. D. C. CRANMER, B. J. HOCKEY, S. M. WIEDERHORN and R. YECKLEY, *Ceram. Engng. and Sci. Proc.* **12** (1991) 1862.

Received 28 October 1991
and accepted 16 January 1992